JOURNAL OF APPLIED ELECTROCHEMISTRY 23 (1993) 141–150

Effect of added polymer traces in crystal growth: electrochemical simulation

C. DESLOUIS

UPR15 du CNRS, Physique des Liquides et Electrochimie, Université Paris VI, Tour 22, 4 Place Jussieu, 75252 Paris Cedex 05, France

F. LEFAUCHEUX, M. C. ROBERT

Laboratoire de Minéralogie-Cristallographie, associé CNRS, Universités Paris VI et Paris VII, Tour 16, 4 place Jussieu, 75252 Paris Cedex 05, France

C. RINAUDO

Dipartimento di Scienze della Terra – Sezione di Mineralogia, Via Valperga Caluso 37, 10100 Torino, Italy

Received 25 November 1991; revised 1 May 1991

Crystals grown in convective media often show defects related to solution flux. Traces of polyethylene oxide (PEO) added to potash alum crystal growth solution slightly reduce the growth rates but significantly improve the quality of the crystal. In order to interpret this action, an electrochemical simulation of mass transfer during growth was attempted. It has been shown that the PEO additive does not act as drag reducer but is adsorbed at the interface, forming a porous filter through which chemical species diffuse.

1. Introduction

Traces of foreign materials are frequently used in solution crystal growth in order to change morphology [1] and to inhibit or promote [2] nucleation. Impurities can be either inorganic ions [3] or organic materials [4] acting on mineral or organic crystals. Fundamental studies on thermodynamics and kinetics of impurity adsorption have been well reviewed [5]. The activity of additives may also be investigated through modification of fluid properties, surface tension or hydrodynamic parameters; this suggests investigation of hydrodynamic drag reducers such as polyethylene oxides [6]. Preliminary experiments were very promising but interpretation was missing. This is the purpose of this paper.

2. Growth defects related to hydrodynamics

Large solution grown monocrystals are usually obtained from seeds which are slices cut from the best part of mother crystals. A classical procedure consists in polishing and cleaning up these slices before fixing them on holders which rotate in a supersaturated solution. The crystal growth rate has been shown to depend on the angular velocity and therefore to be mass transfer limited [8].

Each step of this procedure may induce growth defects as shown on an X-ray topograph of a slice cut out of a potash alum crystal (Fig. 1). The seed-new crystal interface is marked by strong contrasts C underlining the position of some faces of the seed. These contrasts are denoted by using the name of the corresponding face, for example C_{100} for a (1 0 0) face. They reveal strains due to imperfect joining of lattices on both sides of the interface. These strains are related to trapping of solid and liquid inclusions.

2.1. *Liquid inclusions*

2.1.1. Small inclusions (I_S, Fig. 1) are located everywhere around the seed but most of them are inside the seed close to the interface. They are due to imperfect polishing with remaining scratches or to an overcleaning with local dissolution and edge blunting. Such imperfections are unavoidable but their consequence can be minimized or increased according to the selected growth conditions: a moderate initial supersaturation is generally advisable.

2.1.2. Large inclusions (I_l, Fig. 1) are located at the rear of the seed, i.e. downstream with respect to the solution flux induced by the holder rotation. They lie on the new crystal side interface and, in some cases, at a small distance from the interface. Their occurrence has been related to the presence of recirculating eddies in a separation zone [7] where the solution becomes exhausted. This results in a local depletion of material. The size of these inclusions increases when the supersaturation or the velocity decreases. It is difficult to find a good compromise between the moderate supersaturation required for regular advancement of the whole growth front (suppressing the small inclusions) and a supersaturation large enough to avoid inclusions at the rear part. An attempt may be made to

0021-891X

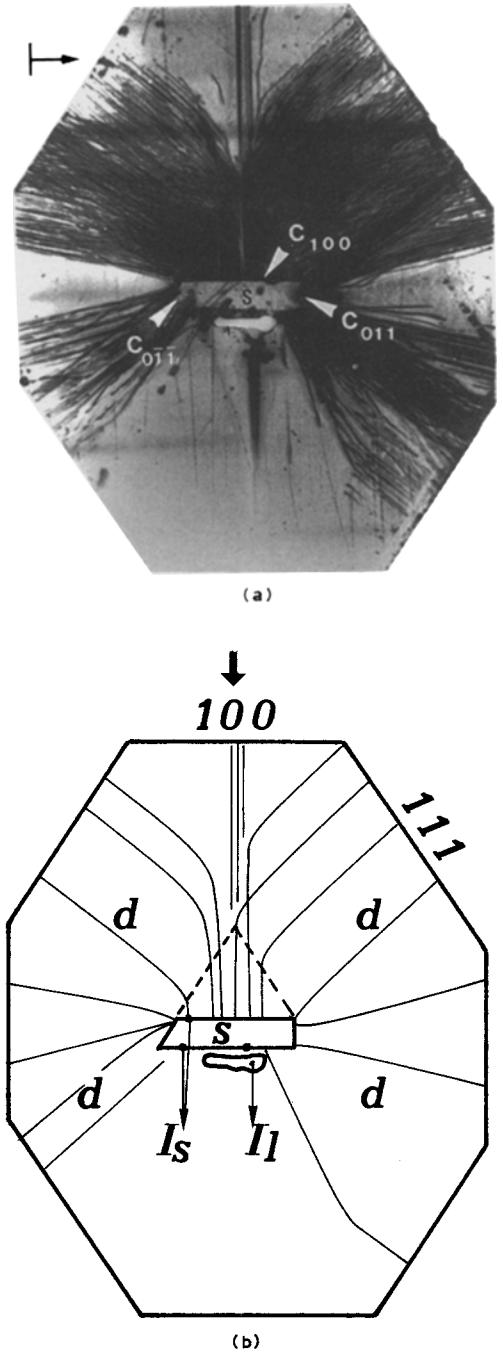

Fig. 1. Growth of a potash alum crystal without additive in a forced convection medium. The thick arrow (b) indicates the direction of the solution flux: flux velocity 6 cm s^{-1}. (a) X-ray topograph of a (0 1 $\bar{1}$) slice cut out of the crystals MoK_α (0 1 1) reflection. (b) A schematic drawing of this topograph showing the main features. *d*: dislocation lines, S: seed, I_l: large liquid inclusions, I_S small liquid inclusions.

prevent stable eddy formation by increasing the solution velocity [7] but this presents other drawbacks as shown in Section 2.2 (below).

2.2. *Solid inclusions*

An optical examination of the front part of the seed sometimes reveals foreign particles such as dust entrapped at the seed-new crystal interface directly exposed to the solution flux [8]. X-ray topography (Fig. 1) shows that these solid inclusions induce strains which are relaxed through the formation of dislocation bundles. Such bundles may also be generated from liquid inclusions. Dislocations are also generated from the parts of the growth front which are apparently inclusion-free: in fact they do contain submicroscopic heterogeneous particles. As the dislocation density increases by increasing the supersaturation or by increasing the solution velocity [9], it has been suggested that theses particles could be secondary nuclei. Secondary nuclei are formed by crystallites pulled out of the seed due to fluid shear stresses [10], and their number increases with increasing supersaturation or solution velocity. All these dislocations propagate up to free surfaces which are either liquid inclusions or, most frequently, the crystal faces (see dislocations *d* in Fig. 1). Such defects generated in the early stages of growth extend over the whole crystal and, consequently, are highly detrimental to the crystal quality. As new defects are seldom generated later on, it is very important to find ways of improving the beginning of growth. In order to modify the hydrodynamic environment, the addition of traces of an additive, a polyethylene oxide, to the growth solution was considered. The results of an exploratory study were encouraging [6] although somewhat surprising: a direct influence of solution hydrodynamics seemed improbable, inhibition or adsorption effects appeared more probable. This paper presents a systematic study of these different aspects. Several additives have been tested: either small molecules of *N*-tetrabutylammonium iodide $In(Bu)_4$ known as an inhibitor in electrocrystallization or macromolecules of polyethylene oxide. The latter are labelled P_2, P_6, P_{30} according to their respective molecular weight 2×10^5, 6×10^5 and 30×10^5. The commercial names of those compounds, as delivered by Union Carbide, are respectively PEO N80, N3000 and WSR 301.

The present study deals with a characterization of crystals obtained with different additives and the modelling of mass transfer in the growth medium through electrochemical investigations.

3. Characterization of crystals grown in the presence of additives

A series of crystals were grown under the same conditions except for the type and amount of additive. The seeds were 100 slices cut from mother crystals. Growth proceeded through the temperature-decrease method at constant rate (0.4 °C day^{-1}). The seeds were rotated in the solution at a constant linear velocity of 6 cm s^{-1}.

3.1. *Growth rates*

The grown crystals were cut normal to the rotation axis of the crystals, leading in this case to (0 1 $\bar{1}$) slices. In such slices, the four octahedral faces {1 1 1}, two cubic faces {0 0 1} and two dodecahedral faces {0 1 0} are normal to the slice plane which made it easy to measure the different growth rates. Figure 2 shows the variation of growth rates as a function of additive contents. As every seed was different in terms of crystal quality, morphology, seed preparation (polishing

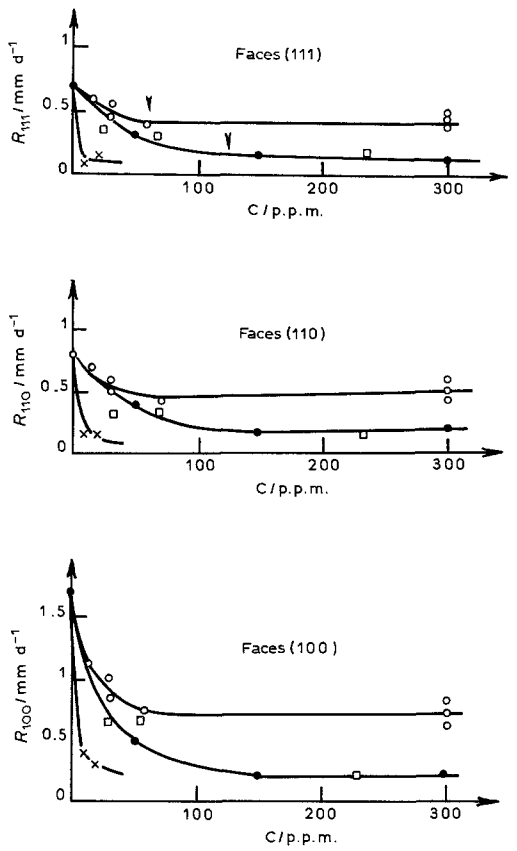

Fig. 2. Growth rates of potash alum crystals as a function of additive concentration, for the different faces: (a) (1 1 1) face, (b) (1 1 0) face, and (c) (1 0 0) face. (○) P_{30}, (●) P_6, (□) P_2 and (×) $In(Bu)_4$.

and cleaning), a growth rate dispersion was observed. The values presented here are averaged from measurements of all the faces of the same type on crystals grown in the same experiment.

In all cases, the addition of $In(Bu)_4$, even in very small quantities, caused a drastic decrease in growth rate for all types of faces.

For the three polymers P_2, P_6 and P_{30}, the growth rates first decreased with additive concentration, then remained unchanged, indicating a saturation effect. The results were plotted according to two curves, the first gathering values of experiments with P_2 and P_6, the other with P_{30}. The minimum concentration required to reach the plateau was higher for the first curve (120 p.p.m.) than for the second (60 p.p.m.) (about 60% of the initial value). Furthermore, the growth rate drop was less pronounced for P_{30} than for P_2 and P_6 (about 15%).

3.2. *Crystal quality*

Figure 3 presents X-ray topographs of slices cut from crystals grown with different additives. In all cases, the front and rear parts of the seed cannot be differentiated in terms of defect distribution, as was the case for the topography presented in Fig. 1. Except for the crystal grown with P_6 (Fig. 3c), the dislocation density generated at the seed–new crystal interface is strongly reduced. Furthermore, the interfaces are highly strained in the case of $In(Bu)_4$ (Fig. 3a) and P_2 (Fig. 3b) which suggests a strong adsorption of additive molecules at the beginning of growth. This is consistent with the strong growth rate decrease observed for a low content of these two compounds.

As far as P_6 is concerned, the crystalline quality is not significantly improved, when using a low additive content (Fig. 3c). Higher contents are required to demonstrate the positive role of the polymer and practically they correspond to the plateau on the growth rate curves (Fig. 2). Figure 3(e) shows an X-ray topography of a crystal grown with 300 p.p.m. of P_6; the seed which lies in the central part is actually indiscernible from newly grown parts.

A high P_{30} content (Fig. 3f) gives results somewhat improved with respect to a lower content (Fig. 3d). Except for the strong contrasts $C_{0\bar{1}\bar{1}}$ and a dense bundle of dislocation d_1, the major part of the seed limit is not easily visible. The dislocations, which are seen in the newly grown crystal, are continuations of dislocations already present in the seed. This is clearly visible for dislocation d_2, which emerges at a seed–new crystal interface marked by a slight contrast (see arrow Fig. 3f). Such prolongations of dislocations from the seed to the new crystal demonstrate the very good joining of crystal lattices of both sides of the interface.

These examples show that use of a suitable content of polyethylene oxide may prevent perturbations, whose effects may extend to the whole crystal. Defects are seldom generated during growth provided growth conditions are kept constant. The main perturbation is generally created when introducing the seed into the growth solution.

4. Mass transfer analysis by electrochemical simulation

The crystal growth experiments only provide an average growth rate for each face. They do not suggest a mechanism for the reduction of the number of dislocations.

To gain a better insight into the modifications of mass transfer close to the solution/crystal interface, an electrochemical experiment yielding an analogy with the crystal growth experiment was performed. This experiment requires a metallic surface as electrode at which a current proportional to the mass transfer rate can be measured. Such a condition is rather different in the crystal growth experiment since the surface is insulating. However, as the polymeric compounds used in the first part are known to present a non selective adsorption of physical nature – coulombic effects – over a large variety of substrates (as shown by ellipsometry in [11]), the conclusions on surface effects from the electrochemical observations will also apply to the crystal growth experiment. As to volume effects, the analogy between the two experiments will be still closer, since the same solutions have been used (saturated potash alum medium).

Mass transport properties were analyzed by using a fast redox reaction (ox + $ne^- \rightleftharpoons$ red) where the measured current due to the exchange of n electrons is proportional either to the transport of oxidized (ox) or

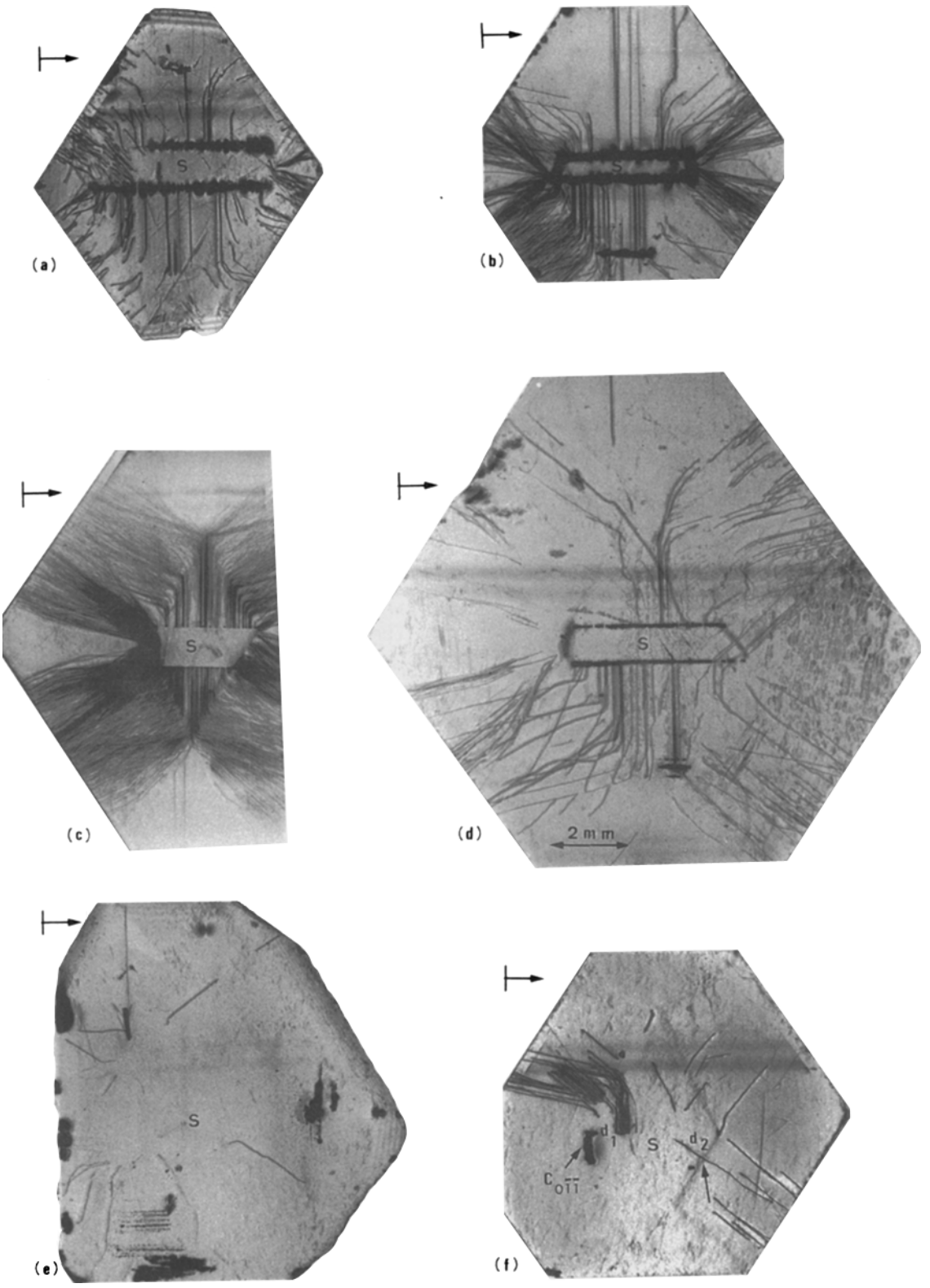

Fig. 3. X-ray topographs of potash alum crystals grown in presence of additives, in the same growth conditions as in Fig. 1. (0 1 $\bar{1}$) slices, MoK_α (0 1 1) reflection, the same scale is used for all the topographs. (a) $In(Bu)_4$: 20 p.p.m. (b) P_2: 70 p.p.m., (c) P_6: 30 p.p.m., (d) P_{30}: 30 p.p.m., (e) P_6: 300 p.p.m. and (f) P_{30}: 300 p.p.m.

reduced (red) species by convective diffusion to or from the surface. Mass transport was quantitatively controlled by using a rotating disc electrode which generates a well-established flow allowing calculation of the mass transfer rate [12, 13].

This flow geometry has the additional advantage of a constant velocity component directed towards the disc surface as the liquid is drawn from infinity along the rotation axis due to the centrifugal action of the disc. This velocity is of order $(\nu\Omega)^{1/2}$ where ν is the kinematic viscosity of the solution and Ω the disc angular velocity. This situation is partially analogous

with the flow conditions in the growth rate experiment, where the relative solution/crystal velocity was $6\,cm\,s^{-1}$.

As none of the ionic species of potash alum present exploitable redox properties in the stability potential range of water, an additional redox couple was added as minor component ($C_b = 10^{-3}$ M) so as to avoid any modification of the ionic medium. The reduction of benzoquinone to hydroquinone ($C_6H_4O_2/C_6H_6O_2$) at a platinum electrode was chosen.

$$O{=}\Phi{=}O + 2e^- + 2H^+ \Rightarrow OH{-}\Phi{-}OH \quad (1)$$

where Φ is the aromatic ring.

The measured current was controlled, in part or completely, by convection/diffusion of benzoquinone towards the electrode surface. Three different types of measurement were carried out.

4.1. *Measurement of the limiting diffusion current*

In the potential plateau region where the benzoquinone concentration is zero at the wall, the limiting current, I_L, is given by the Fick's law:

$$I_L = nFC_b \frac{D}{\delta} A \quad (2)$$

where δ is the diffusion layer thickness [12], given by:

$$\delta \approx 1.61\, D^{1/3}\Omega^{-1/2}\nu^{1/6} \quad (3)$$

where F is the Faraday number ($96\,500\,C\,mol^{-1}$), D the molecular diffusivity, and A the electrode area.

The proportionality of I_L with $\Omega^{1/2}$ is the first criterion of a purely mass transport control and of a uniform reactivity of the interface.

4.2. *Measurement of the a.c. impedance*

This method is based on a frequency analysis of the current response to a sinusoidal potential modulation of low amplitude [13]. The measurements are performed below the limiting current, where the control is partly under mass transport and partly under electron transfer (mixed kinetic conditions). In such conditions, the electrical behaviour of the interface is correctly represented by the equivalent circuit displayed in Fig. 4(a) with its frequency dependence in the complex plane shown in Fig. 4(b). R_T is the charge transfer resistance, defined as $(\delta i/\delta E)_C^{-1}$.

Z_D is the convective diffusion impedance which is proportional to $(di/dC)_{y=0}$. R_E is the electrolyte resistance and C_D is the double layer capacitance.

In the present case, the a.c. impedance diagrams have been only considered in the high frequency range, dominated by the R_T/C_D elements. In the absence of kinetic modifications (as is the case here), the variations of R_T and C_D are only ascribable to adsorption processes.

4.3. *Measurement of the electrohydrodynamic (EHD) impedance*

Electrohydrodynamic impedance measurement involves analysing, with frequency, the response of the limiting current to a sine wave modulation of Ω around a mean value $\bar{\Omega}$ such that $\Omega = \bar{\Omega}(1 + \varepsilon\cos\omega t)$ with $\varepsilon = 0.1$. In particular, the surface may be assumed to be ideally and uniformly active when the EHD impedance depends only on the reduced frequency $p = (\omega/\bar{\Omega})\, Sc^{1/3}$, where Sc is the Schmidt number defined as the ratio of the viscosity, ν, to the diffusivity D [14, 15]. The frequency analysis of the experimental diagrams, by use of the theoretical expression for the impedance, allows determination of the diffusivity when the interface is ideally active, and also to analysis of the deviations with respect to ideality [16].

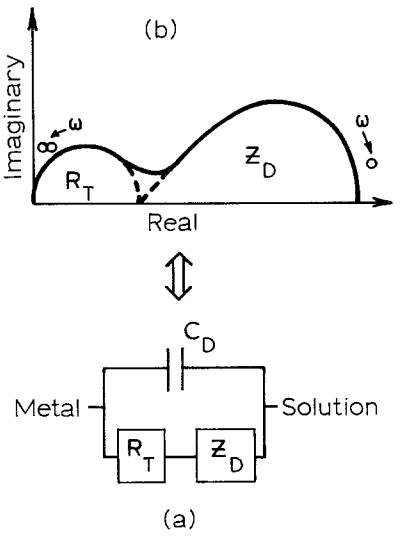

Fig. 4. (a) Electrical equivalent circuit of the metal–electrolyte interface. C_D is the double layer capacity. R_T the charge transfer resistance and Z_D the diffusion impedance. (b) Frequency dependence of the equivalent circuit in (a) in the complex plane (Nyquist diagram).

Experiments were carried out by means of a rotating disc electrode. The angular velocity was controlled between 0 and 5000 r.p.m. with a superimposed modulation at a frequency between 0 and 100 Hz.

The electrode was the cross-section ($0.2\,cm^2$) of a platinum cylinder, the lateral area being protected from the solution by an epoxy insulating sheath. Current–potential curves were recorded with a potentiostat and a three-electrode a.c. cell. EHD impedances were analysed by use of a frequency response analyser (Solartron 1170). Experimental details have been described earlier [17].

5. Results

The measurements were carried out by adding to the electrolytic medium the different compounds used in the first part of this study at concentrations above the threshold values determined in Fig. 2. The compounds are listed below.

PEO	WSR 301	(P_{30})	(30 p.p.m.)
PEO	N 3000	(P_6)	(100 p.p.m.)
PEO	N 80	(P_2)	(300 p.p.m.)
$In(Bu)_4$			(100 p.p.m.)

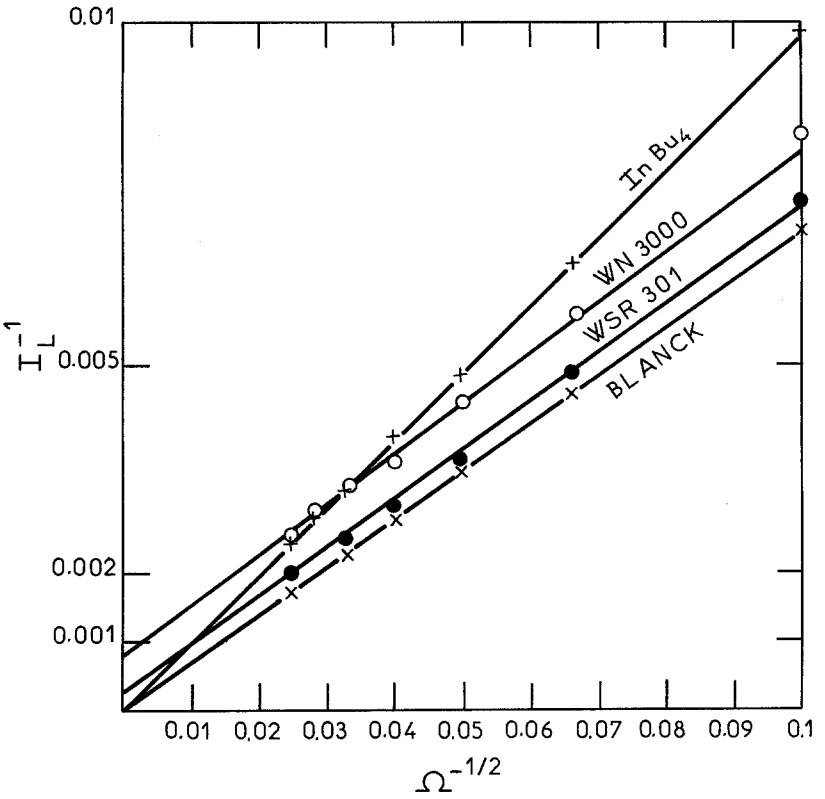

Fig. 5. Koutecky–Levich plots (reciprocal limiting diffusion current against the reciprocal square root of the angular velocity of the disc electrode) for the reduction current of benzoquinone (10^{-3} M) in a saturated potash alum solution containing different additives.

5.1. *Steady-state limiting currents*

Limiting currents I_L reported as a function of $\Omega^{1/2}$ show that the mass fluxes in the presence of additives are systematically lower than in the blank solution (i.e. without additives).

As the $I_L/\Omega^{1/2}$ curves of the PEO series are nonlinear and show a concavity directed downwards, the data have been plotted in reciprocal coordinates I_L^{-1}, $\Omega^{-1/2}$ (Fig. 5) which may prove appropriate in such a case [18]. When the data in these new coordinates – known as Koutecky–Levich plots – fall on a straight line, i.e. follow the equation $I_L^{-1} = \alpha\Omega^{-1/2} + \beta$, several causes can be invoked, either a partial blocking of the interface [19], or the presence of a porous layer adherent to the metal [18], or the existence of a coupling with a chemical reaction (CE mechanism) of first order [12]. For each of those situations, the couple (α, β) contains information relative to either the active fraction of the surface and the characteristic size of the active sites, or the thickness of the porous layer and the diffusivity through it, or the rate constants of the chemical reaction.

In fact, one then observes that the data corresponding to the PEO additives give linear plots parallel to the blank solution line which obviously crosses the coordinate origin: this behaviour may be due to any of the different causes listed above. However, there is here no chemical reason to consider the CE mechanism.

In contrast, the data for $In(Bu)_4$ give a linear plot in Fig. 5 crossing the coordinate origin but with a higher slope than for the blank solution. This situation with $\beta = 0$ can be interpreted in terms of a partial blocking of the interface leaving bare only a small area for electron transfer. This result is consistent with the observed decrease of the growth rate of the crystals when the PEO molecular weight is decreased (see Fig. 2).

For the PEO series, the high permeability values estimated in Fig. 5 explain why the mass fluxes are not significantly lower with respect to the blank solution. In contrast to the steady-state measurements, impedance measurements yield qualitatively different diagrams (especially the EHD impedance), and these have been used to gain information about the action of the polymers.

5.2. *A.c. impedance measurements*

The measurements were performed at the same half-wave potential (i.e. for $I = I_L/2$) for all additives so as to allow quantitative comparisons. For example, an a.c. impedance diagram over the whole frequency range is presented in Fig. 6. The diagram shape compares very well with that expected as shown in Fig. 4(b). The values of the discrete elements of Fig. 4(a) were obtained by fitting the impedance expression corresponding to the electrical equivalent circuit of Fig. 4(a) with the data for all additives and R_T and C_D as reported in Table 1 for $\bar{\Omega} = 600$ r.p.m. Another set of measurements performed at $\bar{\Omega} = 2000$ r.p.m., not reported here, shows qualitatively the same trends.

5.2.1. PEO additives. R_T and C_D both increase and decrease monotonically, respectively, when the molecular weight decreases. This result can be explained by

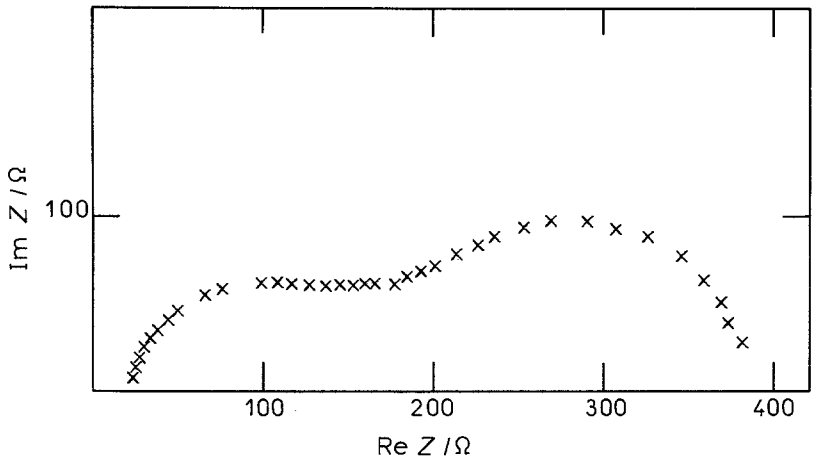

Fig. 6. A.c. impedance diagram performed at the half-wave potential (such that $I_1 = I_l/2$) of the reduction wave of the benzoquinone in the blank solution. Ω = 600 r.p.m.

adsorption depending on an increasing number of bonds between the polymer and the surface, and an increasing concentration of monomers close to the surface. Indeed, as the kinetics of electron transfer are not modified, the increase in R_T is only ascribable to a small reaction area.

5.2.2. In(Bu)$_4$. R_T increases only slightly, revealing a moderate blockage of the reactive area, while the strong decrease of C_D substantiates the highly hydrophobic effect of the butyl radicals. It is worth noting that P_6 and In(Bu)$_4$, which have similar effects on the average mass flux, also increase R_T by the same amount.

5.3. *EHD impedance measurements*

As predicted by the theory, the data can be put on a single diagram as a function of the dimensionless frequency $\omega/\bar{\Omega}$, when the system is completely under convective diffusion control and the surface is ideally active. This is actually observed for the blank solution, as shown in Fig. 7, where the phase shift data measured at $\bar{\Omega}$ = 120 or 900 r.p.m. are gathered on a single curve.

In contrast, with additives, a slight but significant separation of the diagrams occurs when the mean angular velocity is changed, as shown for example in Fig. 8 for the PEO P_{30}. The PEO P_2 only gives perfectly identical diagrams for two different $\bar{\Omega}$ values. With other additives, the diagrams are shifted towards lower p values when $\bar{\Omega}$ is increased. This behaviour was shown to be consistent wtih a partial control by molecular diffusion through a porous film at the wall [18]. A theoretical expression of the EHD impedance, Z_{EHD}, was proposed but the observed shifts are too slight to allow a quantitative determination of δ_f^2/D_f and only a qualitative conclusion can be drawn.

Table 1.

Additive	*Blank*	P_{30} *30 p.p.m.*	P_6 *100 p.p.m.*	P_2 *300 p.p.m.*	*In(Bu)$_4$ 100 p.p.m.*
$R_T/\Omega\,cm^{-2}$	200	206	235	304	230
$C_D/\mu F\,cm^{-2}$	27	26.6	20	7	3.6

6. Discussion

By choosing the different additives for this study, the motivation was to prevent the generation of growth defects, namely the development of dislocations or of liquid inclusions. Some of these defects are related to surface effects since the kinetics of crystallization itself are involved. Other defects, related to volume effects, invoke the presence of eddies generated by the chosen experimental procedure. In(Bu)$_4$, known as a dendrite inhibitor in zinc electrocrystallization [20], was used to test surface effects. The PEO compounds are long chained linear polymers which have remarkable flexibility and have been recognized as being particularly effective as hydrodynamic drag reducers, therefore able to act on volume effects. Let us consider, first, the PEO compounds.

These polymers are known to adopt, depending on the solvent nature, conformations which result from the competition between several processes, Brownian motion, elasticity of the C–C chain, viscous forces, coulombic interactions with ions or dipoles in solution, excluded volume effects. In good solvent conditions, they have the shape of statistical coil, more or less expanded with a gyration radius R_F [21]:

$$R_F = \left[\frac{\tau_Z k_B t}{\eta_S}\right]^{1/3} \tag{4}$$

where k_B is the Boltzmann constant and η_S the solvent dynamic viscosity. The Zimm relaxation time, τ_Z, is the time required for the fully stretched chain to recover its coil shape and is defined by [22]:

$$\tau_Z = \frac{\eta_S[\eta]M}{2.4RT} \tag{5}$$

where M is the molecular weight and $[\eta]$ the intrinsic viscosity which is given by:

$$[\eta] = \underset{C\to 0}{\mathrm{Lt}}\left(\frac{\eta_{solution} - \eta_{solvent}}{\eta_{solvent}} \times \frac{1}{C}\right)$$

where C is the polymer concentration in g cm^{-3}. The

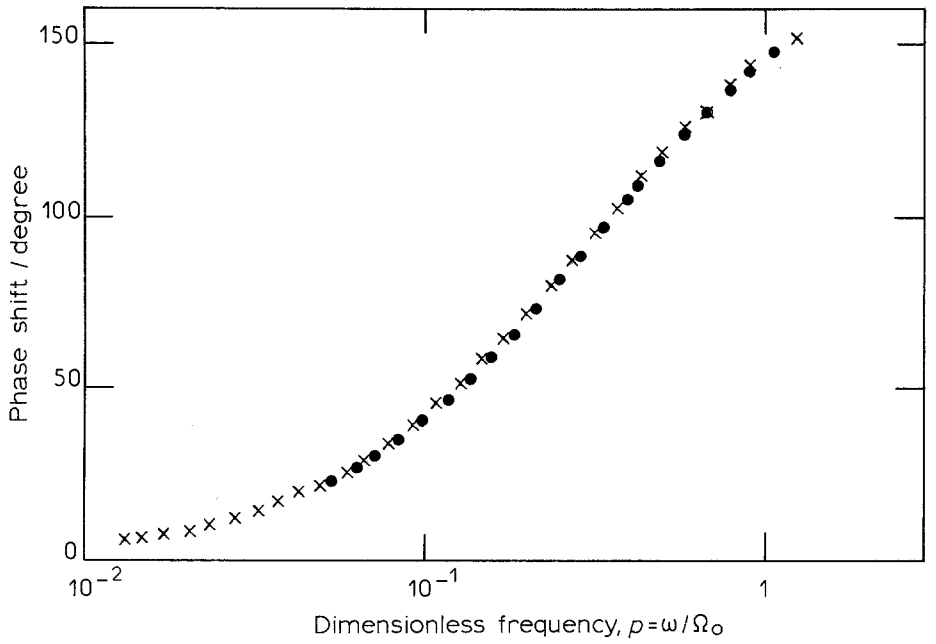

Fig. 7. EHD impedance diagram for the blank solution (saturated potash alum solution and benzoquinone); phase shift as function of the dimensionless frequency $p = \omega/\Omega_0$. Ω_0 = (●) 120 r.p.m; (×) 900 r.p.m. The Schmidt number $Sc = \nu/D$ is 1350.

degree of expansion of the coil and, therefore, its relaxation time, can be determined from $[\eta]$. $[\eta]$ was obtained for increasing potash alum concentrations by measuring the apparent viscosity with a Couette viscometer and by double extrapolation at zero shear rate and at zero polymer concentration.

It can be seen in Fig. 9 that $[\eta]$ remains high ($\geqslant 2000\,cm^3\,g^{-1}$) (which means that the polymer coil remains sufficiently expanded) for potash alum concentrations lower than 0.15 M. When the concentration approaches the saturation value ($C_S \approx 0.240\,3$M), then $[\eta]$ tends to zero. The concentration at the crystal surface in a crystal growth experiment is at least equal to the saturation value and, therefore, the polymer chain would collapse to such a stage as to preclude any hydrodynamic effect. Indeed, hydrodynamic interactions of the polymer coil with the fluid are expected when both time scales, τ_Z and the reciprocal elongational strain rate S^{-1} (s) of the fluid are equivalent, after the analysis of De Gennes [23]. In the growth experiment, S can be roughly estimated as the ratio of the linear relative crystal/solution velocity, U, to the smaller transverse dimension, d, of the crystal. In the best situation, $U/d \approx 150\,s^{-1}$ and $[\eta]$ reaches $2800\,cm^3\,g^{-1}$ at zero concentration in potash alum. Then τ_Z would be around 4.5×10^{-3} s for P_{30} and $\tau_Z \times U/d \approx 0.7$, i.e. somewhat lower than required by the theory. In addition, considering the high concentration values around the growing crystal, any hydrodynamic effect, involving a conformational change of the polymer chains, must be rejected.

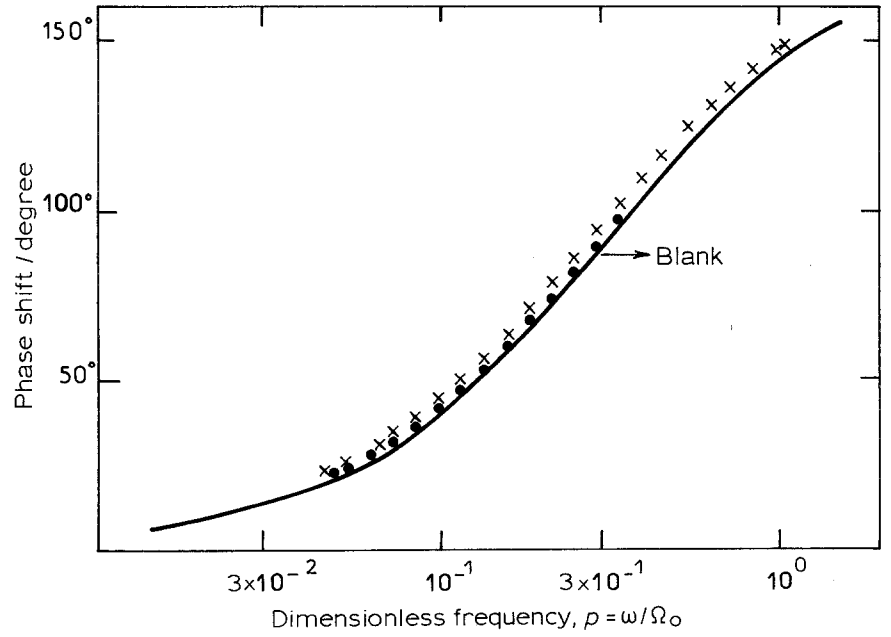

Fig. 8. EHD impedance diagram with PEO WSR 301 (c = 30 p.p.m.). (——) blank solution. (●) 120 r.p.m. and (×) 900 r.p.m.

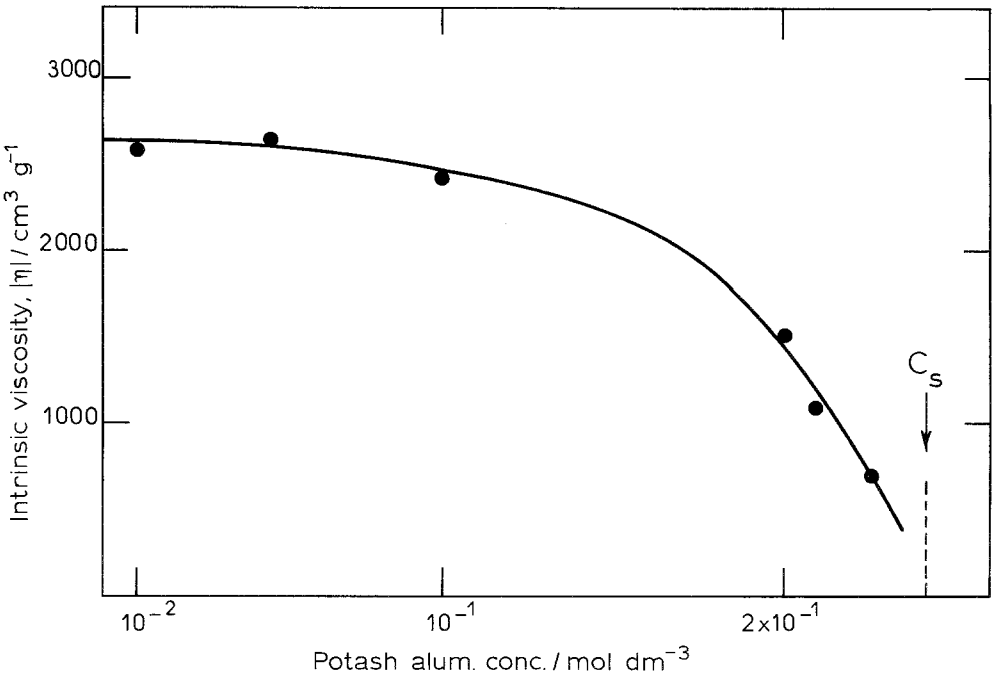

Fig. 9. Instrinsic viscosity $|\eta|$ (in $cm^3 g^{-1}$) of PEO WSR 301 for different potash alum concentrations. $|\eta| = (1/c)|\eta_{solution} - \eta_{solvent}|/\eta_{solvent}$ when $c \to 0$. $\eta_{solution}$ determined at zero shear rate. $C_S = 0.24$ M at 25 °C is the saturation concentration of potash alum.

Therefore, another origin of this effect must be sought. These compounds are also liable to non-specific adsorption [24]. This clearly corresponds to the action mode of $In(Bu)_4$, for which a 2-D adsorption can be invoked. A substantial fraction of the surface is blocked, preferentially the kinks at the origin of dislocations and a two-dimensional – layer by layer – growth mode is favoured. This is not so for the high molecular weight PEO fractions for which R_T was found to be unchanged with respect to the blank and also the growth rate was only slightly reduced.

One possible explanation is that high local supersaturation in potash alum can be maintained in solution close to the surface, so that even though the chains are collapsed, the ions can freely diffuse through this entangled network. This requires that $D_f \approx D$ and that δ_f is small, which is suggested by the EHD experiments.

In addition, the secondary nuclei generated in the bulk which have a larger size cannot reach the crystal surface, since $D_f \ll D$. As they are usually considered as the starting points of new dislocations, this explains the observed effects.

The cumulated effects of polymer adsorption (free diffusion of individual ions, frozen convection and blocking of secondary nuclei) lead to conclusions similar to those drawn from crystal growth in gels [25, 26] with respect to the quality of the final crystal. The definite advantage of the polymer additives is that convection in the bulk maintains a high growth rate.

6. Conclusion

Potash alum crystals grown in solution in the presence of different additives have been systematically characterized: the growth rates of the different faces decrease with increasing additive content down to a limit value. The crystalline quality tested by X-ray topography is improved. The dislocation density is reduced but some liquid and solid inclusions remain. As the chosen additives can act either by adsorption at the interface (case of $In(Bu)_4$) or by reduction of convection in the liquid (usual case of PEO) electrochemical measurements of mass transfer were made. By measuring the a.c. impedance, adsorption processes have been demonstrated. By evaluating the EHD impedance, it has been shown that mass transfer may occur by diffusion through a porous layer. Thus, these additives form a network of polymers, more or less adsorbed at the interface, so that mass transfer towards the crystal occurs only by diffusion.

References

[1] G. M. van Rosmalen and P. Bennema, *J. Cryst. Growth* **99** (1990) 1053.
[2] K. Lewtas, R. D. Tack, D. H. M. Beiny and J. W. Mullin, in 'Advances in Industrial Crystallization', (edited by J. Garside, R. J. Davey and A. G. Jones), Butterworth, Heinemann, London (1991).
[3] C. Rinaudo, M. Franchini-Angela and R. Boistelle, *J. Cryst. Growth* **89** (1988) 257.
[4] S. T. Liu and G. H. Nancollas, *J. Colloïd Interface Sci.* **52** (1975) 593.
[5] A. A. Chernov, in 'Modern Crystallography III', 'Crystal growth', Springer Verlag, Berlin (1984).
[6] F. Lefaucheux, M. C. Robert and C. Deslouis, *J. Cryst. Growth* **53** (1981) 620.
[7] R. Jaussen van Rosmalen and P. Bennema, *ibid.* **42** (1977) 224.
[8] S. Gits Leon, F. Lefaucheux and M. C. Robert, *ibid.* **44** (1978) 345.
[9] S. Gits Leon, M. C. Robert and A. Zarka, *Bull. Soc. Fr. Min.* **101** (1978) 399.
[10] G. D. Botsaris, in 'Industrial Crystallization', (edited by J. W. Mullin), Plenum Press, New York (1976) p. 3.
[11] P. Peyser, R. C. Little and C. R. Singleterry, N.R.L. Report 722 Washington DC. (1971).
[12] V. G. Levich, 'Physicochemical Hydrodynamics', Prentice Hall, Englewood Cliffs, NJ (1962).
[13] D. D. Macdonald, 'Transient Techniques in Electrochemistry', Plenum Press, NY (1977).

[14] C. Deslouis, C. Gabrielli, Ph. Sainte Rose Fanchine and B. Tribollet, *J. Electrochem. Soc.* **129** (1982) 107.
[15] B. Tribollet and J. Newman, *ibid.* **130** (1983) 2016.
[16] C. Deslouis and B. Tribollet, 'Flow Modulation Techniques in Electrochemistry', Advances in Electrochemical Science and Engineering, (edited by Gerisher/Tobias), Vol. 2, VCH, Weinheim (1991) pp. 205–64.
[17] B. Robertson, B. Tribollet and C. Deslouis, *J. Electrochem. Soc.*, **135**, (9), (1988) 2284–2779.
[18] C. Deslouis, B. Tribollet, M. Duprat and F. Moran, *J. Electrochem. Soc.* **134** (1987) 2496.
[19] R. Landsberg and R. Thiele, *Electrochim. Acta* **11** (1966) 1243.
[20] C. Cachet, B. Saidani and R. Wiart, *J. Electrochem. Soc.* **138**, (3), (1991) 678–87.
[21] P. J. Flory, 'Principles of Polymer Chemistry', Cornell University Press, Ithaca and London (1975).
[22] A. Peterlin, *J. Polym. Sci.* **134** (1966) 287–290.
[23] P. G. de Gennes, 'Scaling Concepts in Polymer Physics, Part A, Cornell University Press, Ithaca and London (1979).
[24] P. Peyser and R. C. Little, *J. Polym. Sci.* **18** (1974) 1261–4.
[25] F. Lefaucheux, M. C. Robert, S. Gits, Y. Bernard and B. Gauthier Manuel, *Rev. Int. Hte Temp. Réfract.* **23** (1986) 57–67.
[26] K. Provost, and M. C. Robert, *J. Cryst. Growth* **110** (1991) 258–64.